Numerical Simulation and Experimental Comparison of Channel Geometry on Performance of a PEM Fuel Cell

Iman Khazaee & Mohsen Ghazikhani

Arabian Journal for Science and Engineering

ISSN 1319-8025
Volume 37
Number 8

Arab J Sci Eng (2012) 37:2297-2309
DOI 10.1007/s13369-012-0312-4

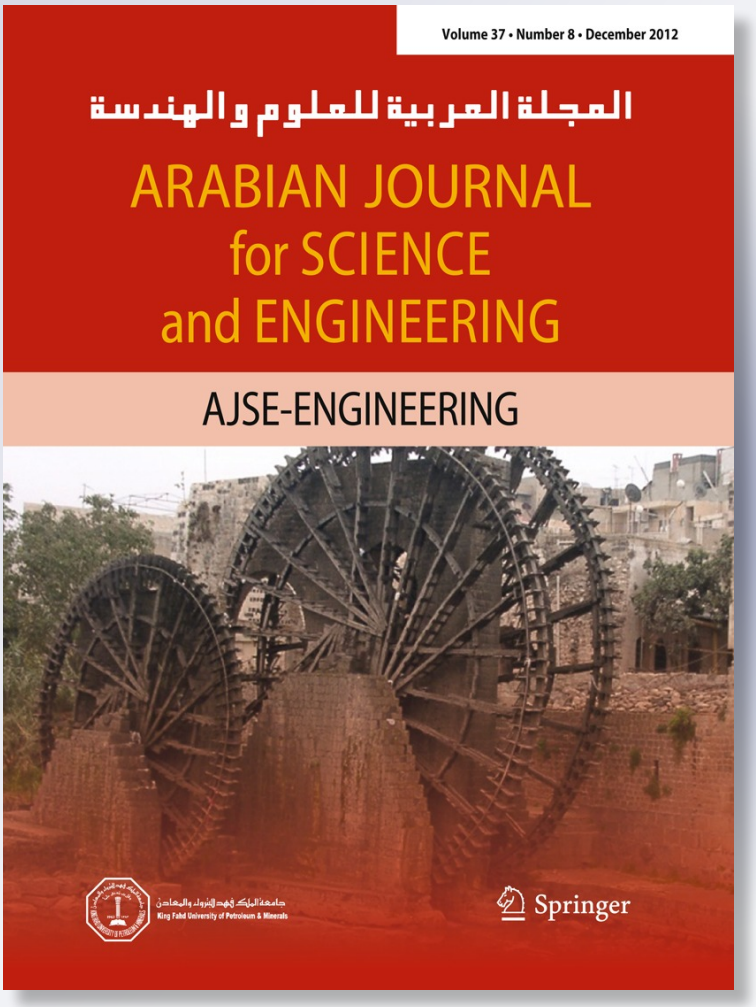

Springer

Arab J Sci Eng (2012) 37:2297–2309
DOI 10.1007/s13369-012-0312-4

RESEARCH ARTICLE - MECHANICAL ENGINEERING

Iman Khazaee · Mohsen Ghazikhani

Numerical Simulation and Experimental Comparison of Channel Geometry on Performance of a PEM Fuel Cell

Received: 4 November 2010 / Accepted: 30 January 2011 / Published online: 10 May 2012

Abstract A complete three-dimensional model for proton exchange membrane (PEM) fuel cells is used to investigate the effect of the channel depth on the performance of the straight flow field at different stoichiometries of air. Therefore, there is a complete cell model that includes all the parts of the PEM fuel cell, flow channels, gas diffusion electrodes, catalyst layers and the membrane. Coupled transport and electrochemical kinetics equations are solved in a single domain; therefore, no interfacial boundary condition is required at the internal boundaries between cell components. This computational fluid dynamics code is used as the direct problem solver, intended to simulate the three-dimensional mass, momentum and species transport phenomena, as well as the electron- and proton-transfer process taking place in a PEMFC. The results show that the predicted polarization curves are in good agreement with the experimental data, and a high performance was observed at the channel depth of 1 mm for the cathode and 1.5 mm for the anode. Furthermore, the results show that the increase of the stoichiometry of air can enhance the performance of the cell. Also, it is observed that the current density distribution is more uniform for channel depth 1 mm for anode and 1.5 mm for cathode and for channel depth 1.5 mm for anode and 1 mm for cathode than the other two designs, and by moving in the channel, mole fraction of oxygen decreases due to consumption.

Keywords PEM fuel cell · Channel depth · Numerical modeling · Cell performance · Polarization · Current density

الخلاصة

يستخدم أنموذج كامل ثلاثي الأبعاد لتبادل غشاء البترول (PEM) لخلايا الوقود، وذلك لدراسة تأثير عمق القناة في أداء مجال التدفق المستقيم عند الـ stoichiometries المختلفة للهواء. ولذلك، هناك أنموذج خلية كامل يشتمل على كل أجزاء خلية الوقود PEM، وقنوات التدفق، وأقطاب انتشار الغاز، وطبقات الحفازات والأغشية. وقد تم حل مجموعة من معادلات الحركة للانتقال والكهروكيميائية في مجال واحد، وبالتالي، لا يتطلب حالة الحد الداخلي بين مكروات الخلية. وقد استخدمت شيفرة حسابات سوائل ديناميكية كحل مباشرة للمشكلة تهدف إلى محاكاة ثلاثية الأبعاد للكتلة، والزخم وظاهرة أنواع الانتقال، بالإضافة إلى عملية انتقال الإلكترون، والبروتون في الـ PENFC وقد أظهرت النتائج أن منحنيات الاستقطاب المتوقعة كانت على اتفاق جيد مع البيانات التجريبية، كما تمت ملاحظة أداء عالٍ عن عمق قناة 1 مم للكاثود و 1.5 مم للأنود. وعلاوة على ذلك، فقد أظهرت النتائج أن stoichiometry للهواء يمكن أن يعزز أداء الخلية، كما لوحظ أيضاً أن شدة توزيع التيار كان أكثر انتظاماً لعمق القناة 1 مم للأنود و 1.5 للكاثود ولعمق قناه 1.5 مم للانود و 1 مم للكاثود اكثر من التصميمين الآخرين. وبوساطه الحركه في القناه فإن الكسر الجزيئي للاكسجين يقل بسبب الاستهلاك.

I. Khazaee (✉) · M. Ghazikhani
Engineering Faculty, Mechanical Engineering Department, Ferdowsi University of Mashhad,
P.O. Box 9177948944-1111, Mashhad, Iran
E-mail: imankhazaee@yahoo.com

I. Khazaee
Department of Mechanical Engineering, Torbat-e-jam branch, Islamic Azad University,
Torbat-e-jam, Iran

List of Symbols

A	Superficial electrode area, m^2
C	Molar concentration, mol/m^3
D	Species diffusivity, m^2/s
i	Current density, A/cm^2
i_0	Reference current density (A/cm^2)
U	Inlet velocity, m/s
j	Transfer current density, A/cm^3
$\vec{u}$	Velocity vector, m/s
P	Pressure, Pa
S	Stoichiometry of air
T	Temperature, K
η	Overpotential, V
ρ	Density, kg/m^3
ε	Porosity
σ	Ionic conductivity, S/m
ϕ	Phase potential, V
ν	Volumetric flow rate, m^3/s
ξ	Water content of the membrane
μ	Viscosity, kg m/s
α	Transfer coefficient for the reaction

1 Introduction

A fuel cell is an electrochemical energy device that converts the chemical energy of fuel directly into electricity and heat, with water as a by-product of the reaction. Based on the types of electrolytes used, they are categorized into polymer electrolyte membrane fuel cells (PEMFCs), solid oxide fuel cells (SOFCs), phosphoric acid fuel cells (PAFCs), molten carbonate fuel cells (MCFCs) and direct methanol fuel cells (DMFCs). The polymer exchange membrane fuel cell (PEMFC) is considered to be the most promising candidate for electric vehicles by virtue of its high power density, zero pollution, low operating temperature, quick start-up capability and long lifetime. PEMFC can also be used in distributed power systems, submarines, and aerospace applications as discussed by Larminie and Dicks [1].

The single-cell PEMFC consists of a carbon plate, a gas diffusion layer (GDL), a catalyst layer, for each of the anode and the cathode sides, as well as a proton exchange membranes (PEM) membrane at the center.

Flow channel geometry is of critical importance for the performance of fuel cells containing PEM, but is of less concern for SOFCs. The reactants, as well as the products, are transported to and from the cell through flow channels. Flow field configurations, including parallel, serpentine, interdigitated and other combined versions, have been developed.

The performance of the fuel cell system is characterized by the current–voltage curve (i.e. polarization curve). The difference between the open circuit potential of the electrochemical reaction and cell voltage occurs from the losses associated with the operation. The corresponding voltage drop is generally classified in three parts:

i. activation overpotential caused by the electrochemical reactions,
ii. ohmic drop across the polymer electrolyte,
iii. mass transfer limitations of reactants

These associated losses dominate over different current density ranges. For low current densities, the activation overpotential is dominant. For high current densities, which are of particular interest for vehicle applications because of higher power density, the mass transfer limitations dominates the losses. For moderate current densities, the ohmic drop across the polymer membrane dominates. Moreover, for high current densities, water starts to exist in liquid form leading to a two-phase transport of reactants to reaction site, which is an additional transport phenomenon of PEM fuel cell operation.

Khazaee and Ghazikhani [2] proposed a complete three-dimensional and single phase model for annular-shaped PEM fuel cell to investigate the effect of using different connections between bipolar plate and GDL on the performances, current density, and temperature and gas concentration. They found that the cell

performance increased as the number of connections between GDL and bipolar plate increased, but for one connection conditions the effect of changing the location of connection on cell performance was negligibly small. Also, they found that the water mole fraction gradually increases along the cell and the maximum of it is near the connections between GDL and bipolar plate.

Chiang and Chu [3] investigated the effects of transport components on the transport phenomena and performance of PEM fuel cells by using a three-dimensional model. The impacts of channel aspect ratio (AR) and GDL thickness were examined. It was found that a flat channel with a small AR or a thin GDL generates more current at low cell voltage due to the merits of better reactant gas transport and liquid water delivery. Also, they found that increase in the anode overpotential and the gas porosity would result in an increase in the current density, especially at low levels of CO concentration.

It was shown in several studies of Meng and Wang [4] and Sivertsen and Djilali [5] that the local electrochemical reaction of the PEM fuel cell as well as the current density exhibits high non-uniformity throughout the entire domain. Also, they found that substantially different spatial distribution can be obtained by varying the asymmetry parameter with no noticeable change in the global current density and polarization curve.

Perng and Wu [6] used a projection finite element analysis with an element-by-element preconditioned conjugate gradient method to investigate the non-isothermal tapered flow channel installed with a baffle plate for enhancing cell performance in the cathodic side of a PEM fuel cell. They studied and explored the parameters including tapered ratio (0.25–1) and gap ratio (0.005–0.2) on the cell performance. They found that the stronger composite effect of tapered flow channel and baffle blockage provides a better convection heat transfer performance and a higher fuel flow velocity to enhance the performance.

Gurau et al. [7] developed a half-cell model to deal with the transport phenomena at the cathode of the PEMFC. The research explored the effects of the porosity of the GDL on the performance of fuel cells. Also, they assumed that the overpotential was constant across the catalyst layer. We will see that this assumption does not hold for the active anode layer and hence the model is not valid for the anode side.

Berning and Djilali [8] used a three-dimensional physical model to evaluate the performance of the fuel cells at different operating conditions. Their research showed that an increase in the fuel cell temperature could raise the cell exchange current density, ionic conductivity of PEM, gas diffusivity and the operating voltage, and then lead to an increase in the cell performance.

Based on the available literature, the present study numerically investigated the effect of such parameters as channel depth and stoichiometry of air on the performance and voltage losses of a PEM fuel cell. Then the study compared the above results with the experimental results of Miansari et al. [9]. The objective of the current work is to show the differences between the results of the modeling and those of the experiments concerning the performance of a PEM fuel cell at different operating conditions and channels depth and the local current density, oxygen mole fraction and water content of membrane distribution that cannot be investigated experimentally.

2 Numerical Model

Cathode electrochemical reactions produce a large amount of liquid water at low operating voltages. If the liquid water is not properly removed and accumulates in the pores of the porous layers, it restricts the oxygen transport to the GDL and the catalyst layer, thereby reducing the electrochemical reaction rate.

The numerical model for the fuel cell used here includes the anode flow channels, anode GDL, anode catalyst layer, PEM, cathode catalyst layer, cathode GDL and cathode flow channels. Miniature fuel cells with dimensions of 70 mm$\times$50 mm$\times$10.731 mm are considered in this investigation. The thickness of the GDL is 0.33 mm, the catalyst layer is 0.01 mm and the PEM is 0.051 mm. The anode and cathode flow channels are assumed to be parallel with channel and rib widths of 1 mm and 0.8 mm, since the anode flow channel geometry has little effect on cell performance.

The proposed model does not require any internal boundary conditions between the components of PEM fuel cell system. A PEM fuel cell system consists of gas channels, gas diffusers, catalyst layers and a polymer membrane, as shown in Fig. 1.

The different physical properties and transport parameters are incorporated into a single set of governing equations using a single domain formulation. The model aims to study the electrochemical kinetics, current distribution, reactant flow fields and multi-component transport of oxidizer and fuel streams in a multi-dimensional domain. The assumptions made in developing the model are as follows:

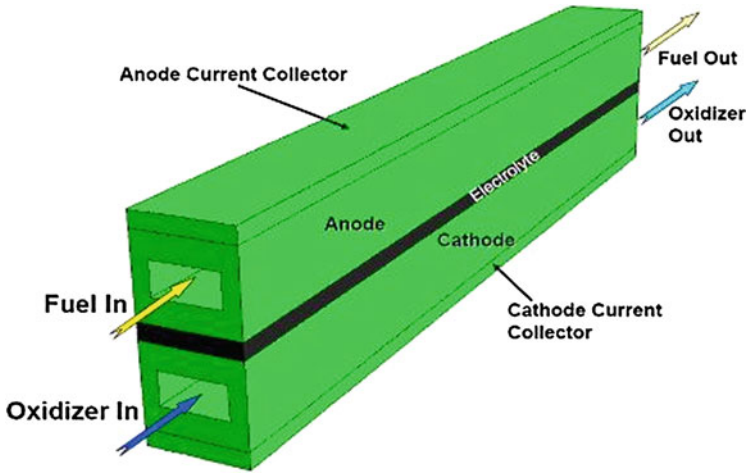

Fig. 1 PEM fuel cell schematics

Ideal gas mixtures
Incompressible and laminar flow because low flow velocities and low fuel utilization
Isotropic and homogeneous porous electrodes, catalyst layers and membrane
Negligible ohmic resistance at porous electrodes and current collectors

The model assumes that the system is steady; the inlet reactants are ideal gases; the flow is laminar; and the porous layers such as the diffusion layer, catalyst layer and PEM are isotropic. The model includes continuity, momentum and species equations for gaseous species, liquid water transport equations in the channels, GDL and catalyst layers, water transport equation in the membrane, and electron and proton transport equations. The Bulter–Volumer equation was used to describe electrochemical reactions in the catalyst layers.

The conservation equations of mass, momentum, species and charge are as follows:

$$\frac{\partial(\rho\varepsilon)}{\partial t} + \nabla.(\varepsilon\rho\vec{u}) = 0 \tag{1}$$

$$\frac{\partial(\rho\varepsilon\vec{u})}{\partial t} + \nabla.(\varepsilon\rho\vec{u}\vec{u}) = -\varepsilon\nabla p + \nabla.(\varepsilon\mu\nabla\vec{u}) + S_u \tag{2}$$

$$\frac{\partial(\varepsilon X_k)}{\partial t} + \nabla\cdot(\varepsilon\vec{u}X_k) = \nabla\cdot(D_k^{\text{eff}}\nabla X_k) + S_k \tag{3}$$

$$\nabla\cdot(\sigma_{\text{g}}^{\text{eff}}\nabla\phi_{\text{e}}) + S_\phi = 0 \tag{4}$$

where $\vec{u}$, X_k and ϕ_{e} denotes intrinsic velocity vector, molar fraction of kth species and electrolyte phase potential, respectively. The corresponding source terms treating the electrochemical reactions and porous media are presented in Table 1.

It is of benefit to further explain the corresponding diffusivities of the governing equations. The diffusivities for species concentration equations and ionic conductivity for membrane phase potential equation are modified using Bruggman correlation to account for porous electrodes, which can be expressed as [10]:

$$D_k^{\text{eff}} = \varepsilon_m^{1.5} D_k \tag{5}$$

$$\sigma_{\text{e}}^{\text{eff}} = \varepsilon_m^{1.5}\sigma_{\text{e}} \tag{6}$$

It is worth further explaining the mole fraction of oxygen appearing in Eq. 3, because oxygen is a gaseous species in the cathode flow channel and gas-diffusion electrode, but becomes a species dissolved in the electrolyte in the catalyst layer and membrane regions. Our definition is given by [10]

$$X_k = \begin{cases} C_k^{\text{g}}/C_{\text{tot}} & \text{in gas} \\ C_k^{\text{e}}/C_{\text{tot}} & \text{in electrode} \end{cases} \tag{7}$$

Table 1 Source terms

	S_v (momenturn)	S_k (species)	S_ϕ (phase potential)	S_n (energy)
Gas channels	0	0	0	0
Backing layers	$-\frac{\mu}{k}\varepsilon^2\overrightarrow{u}$	0	0	0
		$-\frac{ja}{2F}\frac{\rho}{\varepsilon_m\varepsilon_{mc}}$: anode H_2		$\frac{\lvert j_c\rvert}{2F}T\lvert\Delta s\rvert+\lvert j_c\eta_c\rvert$ for cathode and o for anode
Catalyst layers	$-\frac{\mu}{k}\varepsilon^2\overrightarrow{u}$	$\frac{jc}{2F}\frac{\rho}{\varepsilon_m\varepsilon_{mc}}$: cathode O_2		
		$-\frac{jc}{2F}(\frac{1}{2}+n_d)\frac{\rho}{\varepsilon_m\varepsilon_{mc}}$: cathode H_2O	j	
		$-\frac{n_d}{F}ja\frac{\rho}{\varepsilon_m\varepsilon_{mc}}$: anode H_2O		
Membrane	$-\frac{\mu}{k}\varepsilon^2\overrightarrow{u}$	0	0	$\frac{I^2}{k_{mem}}$

where C_k is the molar concentration of species k and superscripts g and e denote the gas and the electrolyte phases, respectively. Thus, X_k is a true mole fraction in the gas phase but is a pseudo mole fraction when species k is in the dissolved form. In addition, there is a discontinuity in the value of X_k at the interface between the gas-diffusion electrode and the catalyst layer due to the following thermodynamic relation [10]

$$C_k^{\mathrm{e,sat}} = \frac{RT}{H}C_k^{\mathrm{g}} \tag{8}$$

where H is the Henry's law constant equal to 2×10^5 atm cm^3/mol for oxygen in the membrane.

Either generation or consumption of chemical species k and the creation of electric current occur only in the active catalyst layers where electrochemical reactions take place. The S_k and S_ϕ terms are therefore related to the transfer current between the solid matrix and the membrane phase inside each of the catalyst layers. These transfer currents at anode and cathode can be expressed as follows [3]

$$j_a = aj_{0,a}^{\mathrm{ref}}\left(\frac{X_{\mathrm{H_2}}}{X_{\mathrm{H_2,ref}}}\right)^{1/2}\left(\frac{\alpha_a+\alpha_c}{RT}\cdot F\cdot\eta\right) \tag{9}$$

$$j_c = -aj_{0,c}^{\mathrm{ref}}\left(\frac{X_{\mathrm{O_2}}}{X_{\mathrm{|O_{2,ref}}}}\right)^{1/2}\left(-\frac{\alpha_c.F}{RT}.\eta\right) \tag{10}$$

The above kinetics expressions are derived from the general Butler- Volmer equation based on the facts that the anode exhibits fast electrokinetics and hence a low surface overpotential to justify a linear kinetic rate equation, and that the cathode has relatively slow kinetics to be adequately described by the Tafel equation. In Eqs. 9 and 10, the surface overpotential, $\eta(x, y)$, is defined as

$$\eta(x, y) = \phi_{\mathrm{s}} - \phi_{\mathrm{e}} - V_{\mathrm{oc}} \tag{11}$$

where ϕ_{s} and ϕ_{e} stand for the potentials of the electronically conductive solid matrix and electrolyte, respectively, at the electrode electrolyte interface. V_{oc} is the reference open-circuit potential of an electrode. V_{oc} is the reference open-circuit potential of an electrode. It is equal to zero on the anode, but is a function of temperature on the cathode, namely [11]

$$V_{\mathrm{oc}} = 0.0025T + 0.2329 \tag{12}$$

where T is in Kelvin and V_{oc} is in volts. Notice that V_{oc} is not the true open-circuit potential of an electrode, which would then depend on reactant concentrations according to the Nernst equation.

Equation 9, which is a rewritten form of the Nernst equation, precisely describes the effect of decreasing transfer current under hydrogen dilution. The dependence of the cathodic exchange current density on temperature can be fitted as [11]

$$\frac{i_0(T)}{i_0(353\ \mathrm{K})} = \exp(0.014189(T-353)) \tag{13}$$

The species diffusivity, D_k, varies in different subregions of the PEMFC depending on the specific physical phase of component k. In flow channels and porous electrodes, species k exists in the gaseous phase, and thus

the diffusion coefficient takes the value in gas, whereas species k is dissolved in the membrane phase within the catalyst layers and the membrane, and thus takes the value corresponding to dissolved species, which is usually a few orders of magnitude lower than that in gas. In addition, the diffusion coefficient is a function of temperature and pressure.

$$D(T) = D_0 \left(\frac{T}{T_0}\right)^{3/2} \left(\frac{p_0}{p}\right) \tag{14}$$

The proton conductivity in the membrane phase has been correlated as [12]

$$\sigma_e(T) = 100 \exp\left[1{,}268\left(\frac{1}{303} - \frac{1}{T}\right)\right](0.005139\xi - 0.00326) \tag{15}$$

where the water content in the membrane, ξ, depends on the water activity, a, according to the following fit of the experimental data [12]

$$\xi = \begin{cases} 0.043 + 17.18a - 39.85a^2 + 36a^3 & 0 \prec a \leq 1 \\ 14 + 1.4(a-1) & 1 \leq a \leq 3 \end{cases} \tag{16}$$

The water activity is in turn calculated by

$$a = \frac{X_{H_2O} p}{p_{sat}} \tag{17}$$

where the saturation pressure of water vapor can be computed from the following empirical equation [12]

$$\ln(p_{sat}) = 70.43464 - \frac{7{,}362.698}{T} + 0.006952T - 9\ln(T) \tag{18}$$

In a fuel cell system, the inlet flow rates are generally expressed as stoichiometry ratio of inlet streams based on a reference current density. The stoichiometry ratios of inlet streams are given by the following equations [1].

$$S^{anode} = C_{H_2} v^{anode} \frac{2F}{i_{ref} A} \tag{19}$$

$$S^{cathode} = C_{O_2} v^{cathode} \frac{4F}{i_{ref} A} \tag{20}$$

Water transport through the polymer electrolyte membrane has been investigated by several researchers in different aspects. Most interesting studies in this area include the determination of water diffusion coefficient and water drag coefficient by Zawodzinski et al. [13,14] and investigation of the diffusion of water in Nafion membranes by Motupally et al. [15].

The electro-osmotic drag coefficient is defined as the number of water molecules transported by each hydrogen proton H^+. The electro-osmotic drag coefficient can be expressed with the following equation:

$$n_d = \frac{2.5\xi}{22} \tag{21}$$

The diffusion coefficient of water in polymer membrane is also highly dependent on the water content of the membrane. The relation is given as:

$$D_w^m = \left\{ \begin{array}{l} 3.1 \times 10^{-7} \xi (\exp(0.28\xi) - 1) \exp(-2346/T) \; 0 \prec \xi \prec 3 \\ 4.17 \times 10^{-8} \xi (1 + 161 \exp(-\xi)) \exp(-2346/T) \; otherwise \end{array} \right\} \tag{22}$$

Once the electrolyte phase potential is determined in the membrane, the local current density along the axial direction can be calculated as follows

$$I(y) = -\sigma_e^{eff} \frac{\partial \phi_e}{\partial x} | x = I.F. \tag{23}$$

where I.F. means the interface between the membrane and cathode catalyst layer. The average current density is then determined by

$$I_{\text{avg}} = \frac{1}{L}\int_0^L I(y)\mathrm{d}y \tag{24}$$

where $L$is the cell length.

There are natural boundary conditions of zero-flux prescribed everywhere other than the inlet and outlets of the flow channels. The boundary conditions prescribed at the inlets of the gas channels are:

$u_{\text{in}}^{\text{anode}} = u_a^0$	$u_{\text{in}}^{\text{cathode}} = u_c^0$
$C_{\text{H}_2}^{\text{anode,in}} = C_{\text{H}_2}^0$	$C_{\text{O}_2}^{\text{cathode,in}} = C_{\text{O}_2}^0$
$C_{\text{H}_2\text{O}}^{\text{anode,in}} = C_{\text{H}_2\text{O}}^{0,a}$	$C_{\text{H}_2\text{O}}^{\text{cathode,in}} = C_{\text{H}_2\text{O}}^{0,c}$

A mesh of 241×74×25 was found to provide required spatial resolution for four-channel geometry. The solution is considered to be converged when the difference between successive iterations is less than 10^{-7} for all variables.

3 Description of the Experiments

The PEM fuel cell system considered in the study of Miansari et al. [9] is a single cell with an active area of 25 cm^2 and straight flow field geometries. The width and land width of the channel were selected to be 1 and 0.8 mm, respectively. The channel depth of 1 and 1.5 mm was considered for experimental and numerical work. For a bipolar plate, non-porous graphite is selected. A Nafion 117 membrane with 4 mg Pt cm^{-2} for the anode and cathode was employed as a membrane electrode assembly. On both sides of the MEA, there were 270-mm thick carbon papers that acted as diffusion layers. The experimental setup is shown in Fig. 2.

Table 2 shows the characteristics of the experimental setup in their study.

The air flow rate was controlled by amass flow controller in the fuel cell test system from Scribner Associate, Inc. The absolute pressure at the air flow inlet and the differential pressure across the whole channel were measured by Omega PX219 and Setra 230 series transducers, respectively. Measurement data from the transducers were real-time displayed and recorded using self-developed Lab-View programs.

The electrochemical and transport parameters used in these simulations are summarized in Table 3, and the operational parameters are presented in Table 4.

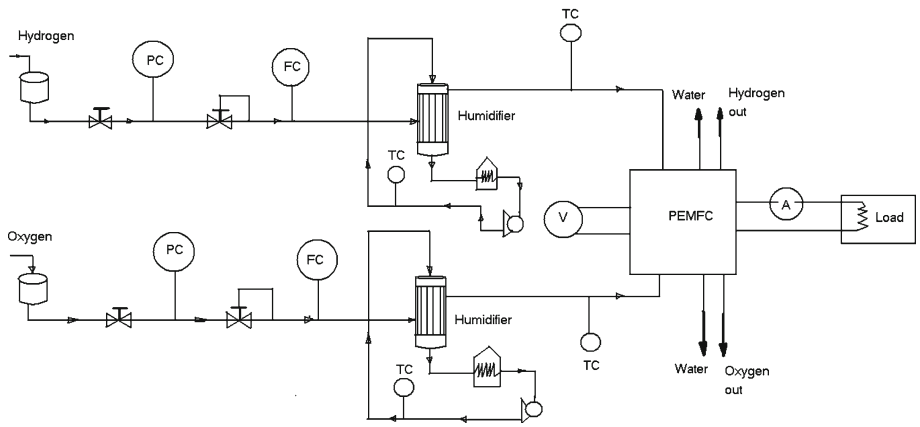

Fig. 2 Single cell with the experimental setup

Table 2 Test setup characteristics

Voltage	0–2 V
Current	0–20 A
Power	0–22 W
Moisture	100 %
Flow rate	0–2 L/min
Gases temperature	Up to 75 °C
Cell temperature	Up to 75 °C

Table 3 Electrochemical and transport properties

Description	Unit	Value
Anode reference exchange current density	A/m^3	1.5e9
Cathode reference exchange current density	A/m^3	4,000,000
Anode transfer coefficient		2
Cathode transfer coefficient		2
Faraday constant	C/mol	96,487
H_2 diffusivity	m^2/s	3e−5
O_2 diffusivity	m^2/s	3e−5
H_2O diffusivity at anode	m^2/s	3e−5
H_2O diffusivity at cathode	m^2/s	3e−5
Anode backing layer porosity		0.5
Cathode backing layer porosity		0.5
Permeability of anode backing layer	m^2	e−12
Permeability of cathode backing layer	m^2	e−12
Equivalent weight of membrane	kg/mol	1.1

Table 4 Operational parameters

Description	Unit	Value
Reference average current density	A/cm^2	1.0
Anode stoichiometric coefficient based on 1.0	A/cm^2	2–4
Cathode stoichoimetric coefficient based on 1.0	A/cm^2	2–4
Anode inlet pressure	Atm	1–3
Cathode inlet pressure	Atm	1–3
Cell temperature	°C	55–35
Anode inlet molar concentration		
Hydrogen	mol/m^3	35.667
Oxygen	mol/m^3	0
Water vapor	mol/m^3	16.121
Cathode inlet molar concentration		
Hydrogen	mol/m^3	0
Oxygen	mol/m^3	7.51
Water vapor	mol/m^3	16.121

4 Results and Discussion

In Fig. 3a–d, the computed polarization curves for different channel depths at the anode side and cathode side are compared to the experimental results at $T = 343$ K, $P = 1$ bar and $S = 2$.

The figures show that the calculated results are in good agreement with the experimental data. The difference between the two curves may be due to the fact that the gas inlet, relative humidity and temperature are fixed in the numerical study, but are flexible in the experiment, which is caused by heat losses along the gas inlet pipes.

Unlike the experimental results, the proposed model is capable of providing more detailed data regarding the operation of fuel cell system, including the flow field, species concentration and current density distribution.

In Fig. 4, the effect of air stoichiometry on the overall cell performance is shown for $P = 1$ bar and $T_{\text{cell}} = 343$ K for three different values of stoichiometry of air. It can be observed that the rise in air stoichiometry enhances the overall performance of the cell as the rise in air stoichiometry increases the molar flow rate of air, which leads to the decrease of cathode overpotential. Also, it is clear that the increase in performance

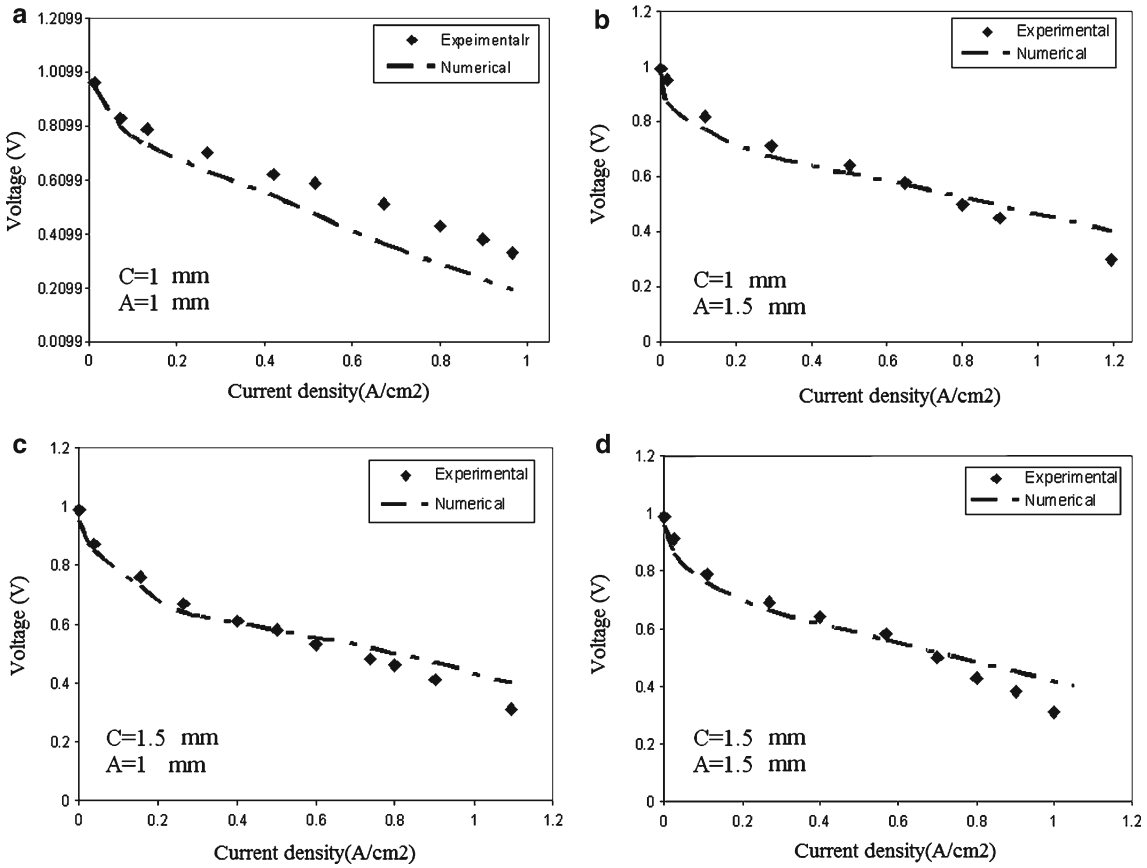

Fig. 3 Validation of numerical cell performance curve with experimental result at different channel depths

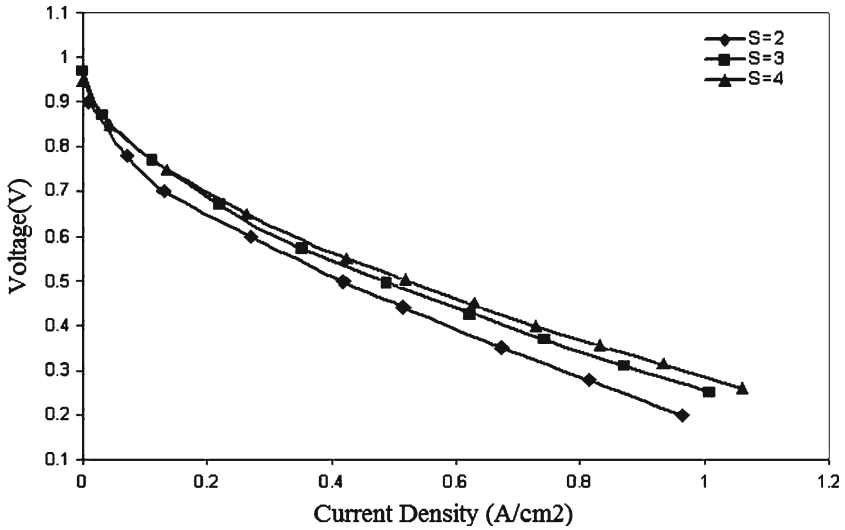

Fig. 4 Variation of cell performance at different stoichiometries of air

for $S = 2$ to $S = 3$ is at lower value than $S = 1$ to $S = 2$ and that it is due to the coming out of the air without electrochemical reaction.

Figure 5 shows the effect of channel depth on cell performance at $T_{\text{cell}} = 343\ K$, $P = 1$ bar and $S = 2$. An overall inspection of Fig. 5 indicates that at the conditions of the higher operating voltage (lower overpotential), the influence of the internal flow modification on the overall fuel cell performance is negligibly small. At lower operating voltage conditions, on the other hand, the effect of the internal flow modification on the polarization

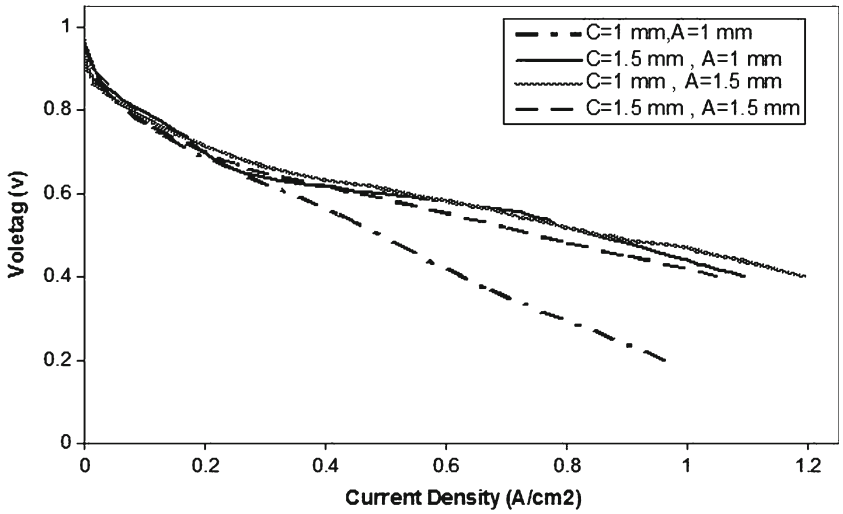

Fig. 5 The effect of channel depth on the cell performance

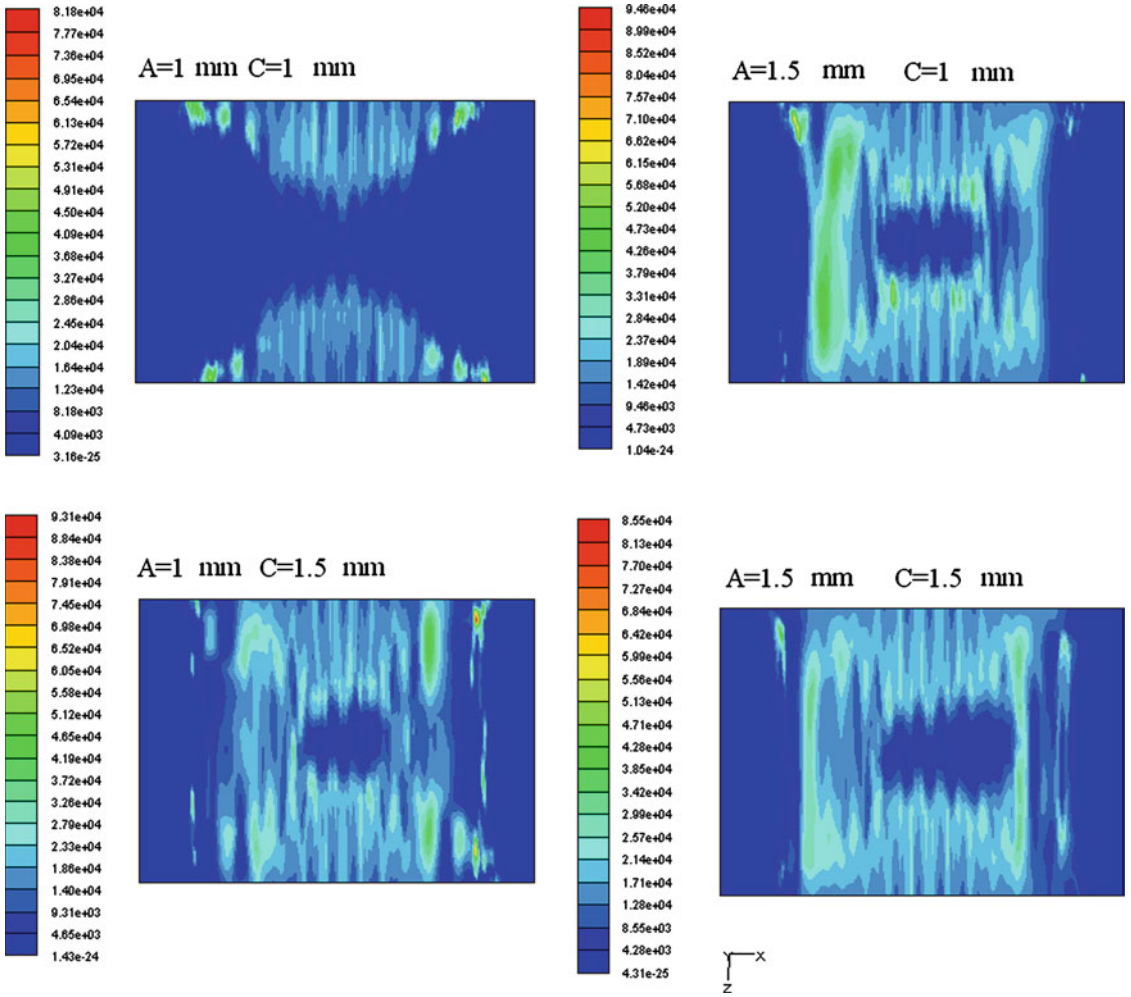

Fig. 6 Current density distribution for four different designs (A/m^2): fully humidified anode and cathode inlets, $V_{\text{cell}} = 0.4$ V and $T = 343$ K

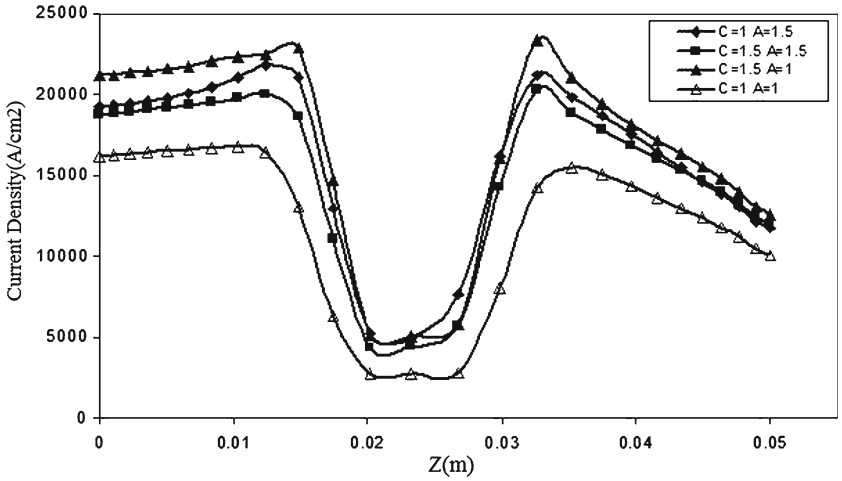

Fig. 7 Local current density distributions at y= 5.33 mm in the middle cross section of cathode catalyst layer surface

curves becomes important. It is clear that the higher performance of the cell is at channel depth of 1.5 mm for anode and 1 mm for cathode, and the performance of the cell is at lower value when the channel depth of anode and cathode sides is 1 mm. Also, it is clear that when the channel depth of the anode and cathode sides decrease, the cell performance decreases due to the decrease in hydrogen consumption and insufficient water removal from the cell.

In Fig. 6, the current density distributions at a cell voltage of 0.4 V and $T_{\text{cell}} = 343\,\text{K}$, $P = 1$ bar and $S = 2$ for four different designs of channel depth are provided. The average current densities are calculated as: 0.6086 A/cm^2 for channel depth of 1 mm for the anode and 1 mm for the cathode, 1.1757 A/cm^2 for channel depth of 1 mm for anode and 1.5 mm for cathode, 1.2109 A/cm^2 for channel depth of 1.5 mm for the anode and 1.5 mm for the cathode, and finally 1.3285 A/cm^2 for channel depth of 1.5 mm for anode and 1 mm for cathode.

It is seen that there is almost 86 % increase in the cell performance when the channel depths of anode and cathode increase from 1 to 1.5 mm. When the results are further investigated, it is observed that the current density distribution is more uniform for channel depth of 1 mm for anode and 1.5 mm for cathode, and for channel depth of 1.5 mm for anode and 1 mm for cathode, than the other two designs.

The channel depth has more significant effects on local current density distribution for straight flow fields. Figure 7 shows the current density distribution at $y = 5.33$ mm on the interface between the cathode GDL and the catalyst layer for the straight flow field at different flow channel depths at 0.4 V. The current density gradually increases as we proceed in the z direction in the channel. Then, it decreases to a lower value and has another increase again and decreases at the end of the channel, i.e. due to increase in electrochemical reaction and decrease because of consumption of gases. It is also clear that the current density is at its lowest value for channel depth 1 mm for the anode and 1 mm for the cathode, and for channel depth 1.5 mm for the anode and 1.5 mm for the cathode.

Figure 8 shows the mole fraction of oxygen at the cathode side channel for different channel depths in $x = 33.9$ mm and $y = 5.33$ mm at $T_{\text{cell}} = 343\,\text{K}$, $P = 1$ bar and $S = 2$. It is clear that as we move in the z direction at the channel, the mole fraction of oxygen decreases due to consumption. But the plot in Fig. 8 exhibits a stronger variation of oxygen concentration between channel depth 1 mm for the anode and 1 mm for the cathode and the other channel depth; this is due to the lesser consumption of oxygen at channel depth 1 mm for the anode and 1 mm for the cathode than the other channel depth. Because of the higher oxygen concentration level provided at channel depth 1 mm for the anode and 1 mm for the cathode, the transverse local current density exhibits conduction overpotential to be the dominant mechanism for cell reaction.

The corresponding sub-rib water contents in the membrane at $y = 5.36$ mm, $T_{\text{cell}} = 343\,\text{K}$, $P = 1$ bar and $S = 2$ are shown in Fig. 9. The decrease in channel depth of the cathode and anode side results in the reduction of the membrane water content and increases of proton transport resistance, which significantly reduce cell performance. Waste heat should be effectively removed from the cell to prevent membrane dryout. Also, it is clear that the change of the water content of the membrane is different for channel depth 1 mm for the anode and 1 mm for the cathode from the other channel depth designs, and the water content of the membrane shifts to a lower value at the middle of the membrane surface of the cell.

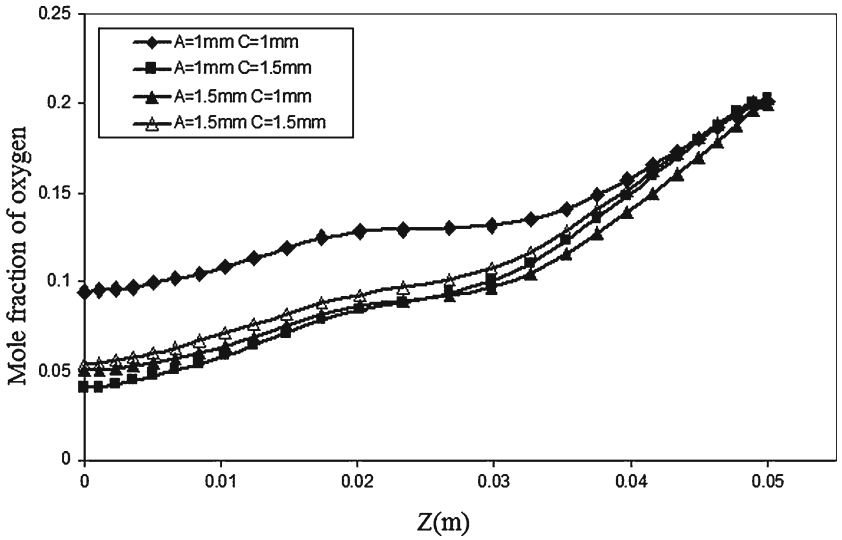

Fig. 8 Transverse oxygen mole fraction at $x = 33.9$ mm and $y = 4.5$ mm with cell voltage of 0.4 V

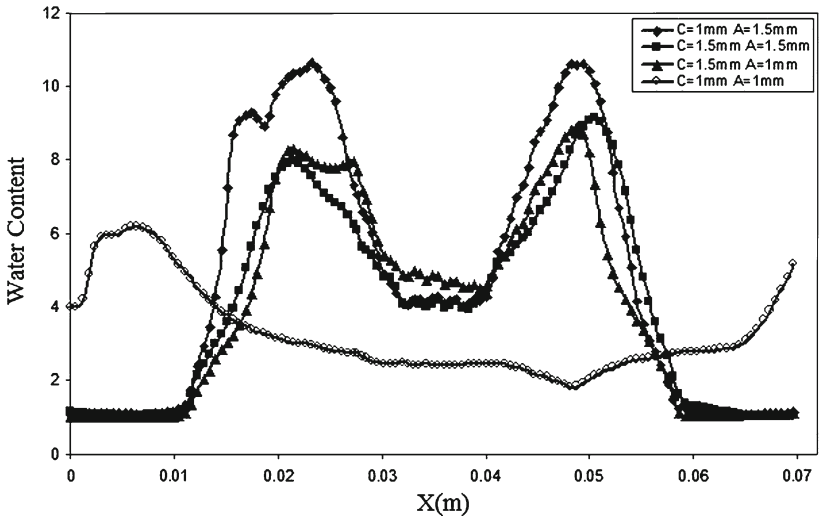

Fig. 9 Water content of membrane along cell width direction for the straight flow field at different channel depths

5 Conclusion

A parametric study is conducted to examine the effect of the varying operating conditions and channel depths on the performance of a PEM fuel cell with dimensions of 70 mm×50 mm×10.731 mm. The complete three-dimensional model for PEM fuel cells based on the two-fluid method was numerically solved with a constant-temperature boundary condition at the surfaces of anode and cathode current collectors. It has been found that:

1. The calculated results are in good agreement with the experimental data.
2. The rise in air stoichiometry enhances the overall performance of the cell, as the rise in air stoichiometry increases the molar flow rate of air, which leads to the decrease of cathode overpotential.
3. The higher performance of the cell is at channel depth of 1.5 mm for anode and 1 mm for cathode, and the performance of the cell is at lower value when the channel depth of the anode and cathode sides is 1 mm.
4. There is almost 86 % increase in the cell performance when the channel depths of anode and cathode increase from 1 to 1.5 mm.

5. The current density gradually increases by moving in the z direction in the channel and then decreases to a lower value, and has another increase again and decreases at the end of the channel; this is due to increase in electrochemical reaction and decrease because of consumption of gases.
6. By moving in the *z* direction at the channel, mole fraction of oxygen decreases due to consumption.
7. The decrease in channels depth of the cathode and anode sides results in the reduction of the membrane water content and the increases of proton transport resistance, which significantly reduce cell performance.

Acknowledgments This work was partially supported by the Renewable Energy Organization of Iran.

References

1. Larminie, J.; Dicks, A.: Fuel cell system explained, 2nd edn. Wiley, New York (2003)
2. Khazaee, I.; Ghazikhani, M.: Performance improvement of proton exchange membrane fuel cell by using annular shaped geometry. J. Power Sour. **196**, 2661–2668 (2011)
3. Chiang, M.S.; Chu, H.S.: Transient behavior of CO poisoning of the anode catalyst layer of a PEM fuel cell. J. Power Sour. **160**, 340–352 (2006)
4. Meng, H.; Wang, C.Y.: Electron transport in PEFCs. J. Electrochem. Soc. **151**, 358–367 (2004)
5. Sivertsen, B.R.; Djilali, N.: CFD based modelling of proton exchange membrane fuel cells. J. Power Sour. **141**, 65–78 (2005)
6. Perng, S.W.; Wu, H.W.: Non-isothermal transport phenomenon and performance of a cathodic with a baffle plate in a tapered channel. Appl. Energy **88**, 52–67 (2011)
7. Gurau, V.; Barbir, F.; Liu, H.: An analytical solution of a half-cell model for PEM fuel cells. J. Electrochem. Soc. **147**, 4485–4493 (2000)
8. Berning, T.; Djilali, N.: A 3D, multi-phase, multicomponent model of the cathode and anode of a PEM fuel cell. J. Power Sour. *124*, 440–452 (2003)
9. Miansari, Me.; Sedighi, K.; Amidpour, M.; Alizadeh, E.; Miansari, Mo.: Experimental and thermodynamic approach on proton exchange membrane fuel cell performance. J. Power Sour. **190**, 356–361 (2009)
10. Bernardi, D.M.; Verbrugge, M.W.: Mathematical model of a gas diffusion electrode bonded to a polymer electrolyte. AICHE J. **37**, 1151–1163 (1991)
11. Parthasarathy, A.; Srinivasan, S.; Appleby, A.J.; Martin, C.R.: Temperature dependence of the electrode kinetics of oxygen reduction at the platinum/Nafion® interface—a microelectrode investigation. J. Electrochem. Soc. **139**, 2530–2537 (1992)
12. Springer, T.E.; Zawodinski, T.A.; Gottesfeld, S.: Polymer electrolyte fuel cell model. J. Electrochem. Soc. **136**, 2334–2342 (1991)
13. Zawodzinski, T.A.; Neeman, J.M.; Sillerud, L.O.; Gottesfeld, S.: Determination of water diffusion coefficients in perfluorosulfonate ionomeric membranes. J. Phys. Chem. **95**, 6040–6044 (1991)
14. Zawodzinski, T.A.; Davey, J.; Valerio, J.; Gottesfeld, S.: The water content dependence of electro-osmotic drag in proton-conducting polymer electrolytes. Electrochimica Acta **40**, 297–302 (1995)
15. Motupally, S.; Becker, A.J.; Weidner, J.W.: Diffusion of Water through Nafion ® 115 membranes. J. Electrochem. Soc. **147**, 3171–3177 (2000)